

**DESIGN AND PERFORMANCE OF LASER
STRUCTURES BASED ON GROUP III-NITRIDES**

SABAH MRESN THAHAB

UNIVERSITI SAINS MALAYSIA

2008

**DESIGN AND PERFORMANCE OF LASER STRUCTURES
BASED ON GROUP III-NITRIDES**

by

SABAH MRESN THAHAB

**Thesis submitted in fulfillment of the
requirements for the degree
of Doctor of Philosophy**

JUNE 2008

ACKNOWLEDGMENTS

I would like to express my sincere gratitude to my main supervisor Associate Professor Dr. Haslan Abu Hassan for his valuable guidance and dedicated support throughout the course of this project, without his patience, guidance and constant supports, this work would not have been possible. I also would like to sincerely thank Associate Professor Dr. Zainuriah Hassan, for additional advice and help. Her valuable advice in many matters is highly appreciated. Thanks also to the offices of Universiti Sains Malaysia Institute for Postgraduate Student, Dean, both deputy Deans and all the staff in the main office of the school of physics. The friendship and assistance from the students at NOR laboratory are also appreciated. I want to give my great honor to my parents, my brothers and my sisters for their support and encouragement.

TABLE OF CONTENTS

Acknowledgments	ii
Table of contents	iii
List of Table	vii
List of Figures	viii
List of Abbreviations	xvi
List of Symbols	xvii
Abstrak	xix
Abstract	xxi
CHAPTER 1– INTRODUCTION	
1.1 Overview	1
1.2 Research Background	11
1.3 Objectives of Study	11
1.4 Out Line of Thesis	12
CHAPTER 2–THEORY	
2.1 Introduction	13
2.2 Background: Semiconductor Laser Theory and Operation	13
2.2.1 Absorption	14
2.2.2 Spontaneous emission	15
2.2.3 Stimulated emission in semiconductors	16
2.2.4 Einstein relations and population inversion	17
2.3 Gain, Losses and the Lasing Condition	18
2.4 Transparency Condition	21
2.5 Differential Gain, Internal Efficiency, External Quantum Efficiency, Differential Efficiency and Output Power	21
2.6 Semiconductor Laser Structures	23
2.7 Coupling Between Optical and Electrical Processes in a Laser diode	26
2.8 Spectrum and Peak Emission Wavelength of Laser Diode	29
2.9 Far-Field Patterns and Beam Divergence of Laser Diode	32

2.10	Quantum Well Laser Diode	33
	2.10.1 Single quantum well (SQW)	34
	2.10.2 Multi quantum wells (MQWs)	35
	2.10.3 Inhomogeneous carrier injection	36
2.11	Construction of a Blue Laser Diode Structure	36
2.12	Quantum Confined Stark Effects and Polarization in LED and LD	39
2.13	Test and Characterization of Laser Diodes	41
	2.13. 1 Determination of principal parameters	41
	2.13.2 Output light versus input current curve and threshold current	41
	2.13.3 Threshold current density	42
	2.13.4 Slope of the illuminance –current ($L-I$) curve	43
	2.13.5 External differential quantum efficiency η_d	44
	2.13.6 Cavity length dependence of the threshold current density and the external differential quantum efficiency	46
	2.13.7 Internal quantum efficiency η_i	47
	2.13.8 Internal loss α_i	48
	2.13.9 Transparency threshold current density	49
	2.13.10 Effect of temperature	49
	2.13.10(a) Characteristic temperature	50
	2.13.10(b) Center wavelength changes with temperature	53
 CHAPTER 3 – SIMULATION METHODOLOGY		
3.1	Introduction	55
3.2	Numerical Simulation Concept	55
3.3	Physical Models	57
3.4	Output Data	61
3.5	Thermal Option	61
3.6	Self-Consistent MQW Option	63
3.7	Definitions	64
	3.7.1 Device modeling	64
	3.7.2 Device simulation	64

3.8	InGaN Laser Diode Simulation Procedure	64
	3.8.1 The fundamental set of equations used in a laser simulation	65
	3.8.2 Coupling between optics and electronics problems	66
	3.8.3 Quantum well transport	68
CHAPTER 4– THE PERFORMANCE OF LASER DIODE STRUCTURES WITH BULK InGaN ACTIVE REGION		
4.1	Introduction	72
4.2	Double Heterostructure Laser (DH) Simulation (Performance and Optimization)	72
4.3	Single Bulk Like Laser Diode Simulation (Performance and Optimization)	80
4.4	Summary	90
CHAPTER 5 – SINGLE AND MULTI QUANTUM WELL LASER DIODE PERFORMANCE		
5.1	Introduction	92
5.2	InGaN Single and Multi Quantum Well with InGaN Barrier Layer	92
5.3	InGaN Single and Multi Quantum Well with GaN Barrier Layer	103
5.4	InGaN Barrier Doped and Thickness Effect	106
5.5	Summary	109
CHAPTER 6– STUDY OF (InGaN/InGaN AND InGaN/GaN) QUANTUM WELL LASER CHARACTERIZATION PARAMETERS		
6.1	Introduction	110
6.2	InGaN Well /InGaN Barrier Laser Diode	111
	6.2.1 The internal quantum efficiency η_i and internal loss α_i	111
	6.2.2 Transparency threshold current density	112
	6.2.3 Characteristic temperature T_0	113
6.3	InGaN Well /GaN Barrier Laser Diode	114
	6.3.1 Laser diode internal quantum efficiency η_i and internal loss α_i	114
	6.3.2 Transparency threshold current density	114
	6.3.3 Characteristic temperature T_0	116

6.3.4	Cavity length effect on the InGaN/ GaN barrier LD performance	116
6.3.5	The optical gain of the DQW InGaN/ GaN barrier LD	119
6.3.6	The internal quantum efficiency, confinement factor and transparency threshold current density as function of InGaN/GaN quantum well number	121
6.3.7	Characteristic temperature T_0 and temperature effect on the performance of InGaN/GaN barrier LD	121
6.4	Summary	125
CHAPTER 7– InGaN MQW LDS DESIGNS OPTIMIZATION, CHARACTERIZATION AND PERFORMANCE ENHANCEMENT		
7.1	Introduction	126
7.2	AlGaIn/GaN Modulation Doped Strained Layer Superlattice (MD SLS) of InGaIn MQW Laser Diodes	126
7.3	Effect of Varying Quantum Well Thickness on the Performance of InGaIn/GaN Single Quantum Well Laser Diode with MD-SLS	139
7.4	The Influences of Using AlGaIn/GaN Multiquantum Stopper Layers on the Performance and Characteristic Temperature of InGaIn/GaN Laser Diodes	146
7.5	Ridge Geometry InGaIn Multi Quantum Well Structure Laser Diode Performance and Characterization	158
7.6	The Performance of InGaIn/InGaIn DQWs Laser Diode Consisting of a Separate Confinement Heterostructure	163
7.7	Influence of Thick n-AlGaIn Contact Layer on the Performance of MD-SLS InGaIn/InGaIn DQWs LD	168
7.8	The Effects of Strained Single Quantum Well on the Performance of InGaIn/GaN Laser Diode	173
7.9	Summary	180
CHAPTER 8 – CONCLUSIONS AND FUTURE WORK		
8.1	Conclusions	184
8.2	Future Works	188
	REFERENCES	190
	PUBLICATIONS	199
	APPENDICES	201

LIST OF TABLES

		Page
Table 2.1	Symbols used in the simplified photon and carrier rate equations.	29
Table 2.2	The typical slope $\Delta p / \Delta I$ and external differential quantum efficiency (DQE) η_d values for lasers with various cavity lengths (Mobarhan, 1999).	48
Table 2.3	The threshold current I_{th} and threshold current density J_{th} values determined for the $L-I$ curves at different temperatures with cavity length $L = 1$ mm and stripe width $W = 100$ μm (Mobarhan, 1999).	53
Table 7.1	A comparison of the output parameters of InGaN with MD-SLS cladding layers and InGaN with bulk cladding layer laser diodes designed in our study.	182
Table 7.2	A comparison of the output parameters of two InGaN laser diode structures with MQBs and EBL stopper layer designed in our study.	183

LIST OF FIGURES		Page
Figure 1.1	Number of publications (INSPEC) and activities in GaN over the years (Akasaki, 2002).	3
Figure 2.1	The mechanism of the spontaneous absorption and emission.	14
Figure 2.2	Process of stimulated recombination in laser diode.	16
Figure 2.3	A schematic description of a Fabry-Perot resonant cavity with reflecting facets on each end.	24
Figure 2.4	Design illustration of edge-emitting and vertical-cavity lasers. (Piprek 2007)	26
Figure 2.5	The emission spectrum of spontaneous and stimulated emission in a Fabry-Perot resonant cavity laser diode.	27
Figure 2.6	The power-current characteristic of a semiconductor laser diode.	27
Figure 2.7	Current step response of (a) photon density, and (b) scaled photon density and carrier density for comparison.	30
Figure 2.8	Typical spectrum of a 1 mm cavity length laser diode operating just above threshold with peak wavelength of emission (λ_p) of 800 nm and the separation between adjacent peaks ($\Delta\lambda$) is about 0.09 nm.	31
Figure 2.9	Effect of increasing operating current (and power) level on the output spectra of multimode gain guided device and single mode index guided device.	32
Figure 2.10	Far and near field pattern and beam divergence of laser diode.	33
Figure 2.11	The single quantum well profile of laser diode.	34
Figure 2.12	The multi quantum wells profile of laser diode.	35
Figure 2.13	The inhomogeneous carrier injection in laser diode active region.	36
Figure 2.14	The structure of InGaN multi quantum well laser diode (Ponce, 1997).	38
Figure 2.15	The AlGaIn current-blocking layer in an AlGaIn/GaN/GaInN multi-quantum well. (a) Band diagram without doping. (b) Band diagram with doping. The Al content in the electron – blocking layer is higher than in the p-type confinement layer.	39
Figure 2.16	Active region band diagram with (rectangle shape) and without (skewed shape) built in polarization at room temperature (Piprek, 2007).	40

Figure 2.17	A typical light versus current (L-I) curve associated with a high power laser diode.	42
Figure 2.18	A typical cavity length dependence of the inverse external differential quantum efficiency (Mobarhan, 1999).	51
Figure 2.19	Typical representation of threshold current density, J_{th} versus the inverse cavity length, $1/L$ for lasers of different cavity lengths, the intercept of the linear fit line of the data points with the vertical axis determines the value of the transparency current density J_0 (Mobarhan, 1999).	51
Figure 2.20	Light versus current characteristic curves for a laser diode operating at various temperatures (Mobarhan, 1999)..	52
Figure 2.21	Graph showing the variations of the natural logarithm of threshold current density $\ln(J_{th})$ with increasing temperature(Mobarhan, 1999).	54
Figure 2.22	The effects of temperature on center emission wavelength of laser diode (Mobarhan 1999).	54
Figure 3.1	ISE tools flow. (Manual of Integrated System Engineering (ISE TCAD) AG, Switzerland)	56
Figure 3.2	Self –consistent solutions provided by ISE simulator. (Manual of Integrated System Engineering (ISE TCAD) AG, Switzerland)	60
Figure 3.3	Time scale for each, quantum mechanical treatment for carriers and classical treatment for optical. (Manual of Integrated System Engineering (ISE TCAD) AG, Switzerland)	60
Figure 3.4	Typical design flow with DESSIS device simulation. (Manual of Integrated System Engineering (ISE TCAD) AG, Switzerland)	65
Figure 3.5	The coupling between optics and electronics problems. (Manual of Integrated System Engineering (ISE TCAD) AG, Switzerland)	67
Figure 3.6	The capture mechanisms inside the quantum well in laser diode. (Manual of Integrated System Engineering (ISE TCAD) AG, Switzerland)	69
Figure 4.1	Schematic diagram of the DH InGaN laser diode structure under study.	73
Figure 4.2	Band diagram and electrostatic potential distribution inside the active region of DH InGaN laser diode.	74
Figure 4.3	The carrier density distribution profile inside DH InGaN laser diode.	75

Figure 4.4	Optical material gain in the InGaN DH LD.	75
Figure 4.5	Laser output power and bias voltage as a function of the forward current of the InGaN DH LD.	76
Figure 4.6	InGaN DH LD mode gain spectrum as a function of energy.	76
Figure 4.7	InGaN DH LD gain spectrum as a function of forward current.	77
Figure 4.8	The emission wavelength as a function of the forward current of InGaN DH LD.	78
Figure 4.9	Optical material intensity of the InGaN DH LD.	79
Figure 4.10	The bandgap energy of the InGaN DH LD with and without graded $\text{Al}_{0.15}\text{Ga}_{0.85}\text{N}$ layer.	79
Figure 4.11	The output power as a function of forward current of DH LD with and without graded $\text{Al}_{0.15}\text{Ga}_{0.85}\text{N}$ layers.	80
Figure 4.12	Schematic diagram of the InGaN laser diode structure under study.	81
Figure 4.13	Band diagram and electrostatic potential distribution for our laser diode structure under study.	82
Figure 4.14	Band diagram, optical material gain and optical intensity for our laser diode structure under study.	82
Figure 4.15	The carrier density distribution profile inside InGaN LD.	84
Figure 4.16	Laser output power of InGaN laser diode structure as a function of forward current at different active layer thickness.	84
Figure 4.17	Laser output power of InGaN laser diode structure as a function of forward current with and without stopper layer.	85
Figure 4.18	Laser output power of InGaN laser diode structure as a function of forward current at different stopper layer thickness.	88
Figure 4.19	Laser output power of InGaN laser diode structure as a function of forward current at different active doping level.	88
Figure 4.20	The far-field pattern of InGaN laser diode in planes parallel and perpendicular to the junction under room temperature.	89
Figure 5.1	Schematic diagram of the preliminary InGaN MQWs LD.	93
Figure 5.2	Energy band diagram of the double quantum well InGaN LD together with electrostatic potential profile.	94
Figure 5.3	Optical material gain in the InGaN double quantum well LD.	94

Figure 5.4	Carriers density distribution profiles in the double quantum well of InGaN LD.	96
Figure 5.5	Optical material intensity of the InGaN double quantum well LD.	96
Figure 5.6	Internal electric field of the InGaN double quantum well LD.	97
Figure 5.7	Electron current density of the InGaN double quantum well LD.	97
Figure 5.8	Laser output power and slope efficiency as a function of the forward current for the double quantum well InGaN LD.	99
Figure 5.9	The emission wavelength and differential external quantum efficiency as a function of the forward current for the double quantum well InGaN LD.	99
Figure 5.10	Laser output power, slope efficiency, threshold current and differential quantum efficiency (DQE) as a function of well number of the MQWs InGaN LD.	101
Figure 5.11	Threshold current density (J_{th}) as a function of quantum wells number obtained by Nakamura experimental work and our simulation work.	102
Figure 5.12	Laser mode gain as a function of forward current for InGaN DQWs LD.	102
Figure 5.13	The output power, threshold current density, slope efficiency and DQE as a function of quantum well number of InGaN LD.	104
Figure 5.14	Carrier density distributed profile in the quantum well for InGaN TQWs LD.	104
Figure 5.15	Optical material gain in the InGaN TQWs LD together with internal electric field.	106
Figure 5.16	Output wavelength of DQWs InGaN/GaN LD as a function of forward current.	107
Figure 5.17	Laser output power, slope efficiency and threshold current as a function of barrier doping concentration.	108
Figure 5.18	Laser output power and threshold current as a function of barrier thickness.	108
Figure 6.1	Inverse of the external quantum efficiency as a function of cavity length of DQWs InGaN/InGaN barrier LD.	112
Figure 6.2	The threshold current density as a function of inverse cavity length of DQWs InGaN/InGaN barrier LD.	112

Figure 6.3	The variations of the threshold current density ($\ln J_{th}$) with increasing temperature of DQWs InGaN/InGaN barrier LD.	113
Figure 6.4	Inverse of the external quantum efficiency as a function of cavity length of DQWs InGaN/ GaN barrier LD.	115
Figure 6.5	The threshold current density as a function of inverse cavity length of DQWs InGaN/ GaN barrier LD.	115
Figure 6.6	The variations of the logarithm threshold current density ($\ln J_{th}$) with increasing temperature of DQWs InGaN/GaN barrier LD.	117
Figure 6.7	The threshold current and the peak wavelength as a function of the cavity length of DQWs InGaN/ GaN barrier LD.	118
Figure 6.8	The output power, slope efficiency and DQE of DQWs InGaN/GaN barrier LD as a function of cavity length.	118
Figure 6.9	The peak mode gain and the total losses as a function of cavity length of DQWs InGaN/GaN barrier LD.	120
Figure 6.10	The mode gain of DQWs InGaN/GaN barrier LD as a function of wavelength at different cavity length value.	120
Figure 6.11	Internal quantum efficiency, transparency current density, threshold current density and confinement factor as a function of quantum well number of MQWs InGaN LD at room temperature.	123
Figure 6.12	Threshold current, peak wavelength and DQE as a function of device temperature of InGaN DQWs LD.	124
Figure 6.13	The variations of the threshold current density ($\ln J_{th}$) with increasing temperature of SQW, DQWs and TQWs InGaN LD.	124
Figure 7.1	Schematic diagram of the preliminary MD-SLS InGaN DQWs LD.	129
Figure 7.2	The conduction band and the valence band profile of MD-SLS InGaN DQWs LD.	131
Figure 7.3	Carrier density distributed profile of InGaN DQWs LD.	131
Figure 7.4	Optical material intensity and the refractive index profile of the MD-SLS InGaN DQWs LD.	132
Figure 7.5	Internal electric field of the InGaN DQWs LD.	132
Figure 7.6	The emission wavelength as a function of the forward current for the DQWs InGaN LD.	133
Figure 7.7	Optical material intensity of InGaN DQWs LD with bulk and MD-SLS cladding layers.	133

Figure 7.8	Total current density profile of InGaN DQWs LD with bulk and MD-SLS cladding layers.	135
Figure 7.9	The output power and bias voltage of MD-SLS InGaN DQWs LD as a function of forward current.	135
Figure 7.10	The output power of MD-SLS and bulk cladding layers of InGaN DQWs LD as a function of forward current.	136
Figure 7.11	The far-field pattern of MD-SLS InGaN DQWs LD.	136
Figure 7.12	The variations of the threshold current density ($\ln J_{th}$) with increasing temperature of MD-SLS and bulk cladding layers of InGaN DQWs LD.	138
Figure 7.13	The threshold current density as a function of inverse cavity length of MD-SLS and bulk cladding layers InGaN DQWs LD.	138
Figure 7.14	Schematic diagram of the preliminary SQW InGaN LDs.	141
Figure 7.15	The conduction band and valence band profile of MD-SLS InGaN SQW LD.	141
Figure 7.16	The variation in the threshold current density as a function of quantum well thickness of MD-SLS SQW InGaN LD.	143
Figure 7.17	The peak wavelength as a function of quantum well thickness of MD-SLS SQW InGaN LD.	143
Figure 7.18	The optical intensity as a function of quantum well thickness of MD-SLS SQW InGaN LD.	144
Figure 7.19	The output power as a function of quantum well thickness.	145
Figure 7.20	The variations of the logarithm threshold current density ($\ln J_{th}$) with increasing temperature of MD-SLS SQW InGaN LD.	145
Figure 7.21	Schematic diagram of the preliminary InGaN DQWs LD.	148
Figure 7.22	Energy band diagram of InGaN DQWs LD with MQBs and EBL.	149
Figure 7.23	Valence band and the conduction band profile of MQWs InGaN LD with MQBs.	149
Figure 7.24	Carrier density distributed profile in the MQWs InGaN LD with MQBs and EBL.	151
Figure 7.25	Optical material intensity and the refractive index profile of the InGaN DQWs LD with MQBs.	151
Figure 7.26	The output power and bias voltage of InGaN DQWs LD with MQBs as a function of forward current.	152

Figure 7.27	The output power of InGaN DQWs LD with MQBs and with EBL as a function of forward current.	152
Figure 7.28	Output wavelength of InGaN DQWs LD with MQBs as a function of forward current.	154
Figure 7.29	The variations of the threshold current density ($\ln J_{th}$) with increasing temperature for MQBs and EBL InGaN LD.	154
Figure 7.30	The peak wavelength and DQE as a function of device temperature for InGaN DQW MQBs LD.	156
Figure 7.31	Inverse of the DQE as a function of cavity length of DQWs InGaN MQBs LD.	156
Figure 7.32	The threshold current density as a function of inverse cavity length of DQWs InGaN MQBs LD.	157
Figure 7.33	The comparison relation between our simulations results with experimental results obtained by Lee et.al(2006)	157
Figure 7.34	Schematic diagram of the preliminary ridge geometry InGaN DQWs LD.	160
Figure 7.35	The optical intensity and the refractive index profile of the ridge geometry InGaN DQWs.	160
Figure 7.36	The output power and bias voltage of ridge geometry InGaN DQWs LD as a function of forward current.	161
Figure 7.37	Inverse of the DQE as a function of cavity length of ridge geometry InGaN DQWs LD.	162
Figure 7.38	The threshold current density as a function of inverse cavity length of ridge geometry InGaN DQWs LD.	162
Figure 7.39	The variations of the logarithm of threshold current density ($\ln J_{th}$) with increasing temperature of gain guide and ridge geometry InGaN DQWs LD.	163
Figure 7.40	Schematic diagram of the preliminary InGaN SCH MD-SLS DQWs LD.	165
Figure 7.41	Bandgap energy profile of SCH MD-SLS InGaN DQWs LD.	165
Figure 7.42	Valence band and the conduction band profile of SCH MD-SLS InGaN DQWs LD.	166
Figure 7.43	The optical intensity and the refractive index profile of the SCH MD-SLS InGaN DQWs LD.	167
Figure 7.44	The output power and bias voltage of MD-SLS InGaN DQW LD as a function forward current.	167
Figure 7.45	The threshold current density as a function of inverse cavity length of MD-SLS DQWs InGaN.	168

Figure 7.46	Schematic diagram of the preliminary MD-SLS InGaN DQWs LD with n-AlGaN contact layer.	170
Figure 7.47	Carrier density distribution profile together with the bandgap energy of MD-SLS InGaN DQWs LD.	170
Figure 7.48	The output power and bias voltage of MD-SLS InGaN DQWs LD as a function of forward current.	171
Figure 7.49	Output wavelength as function of forward current of MD-SLS InGaN DQW LD with n-AlGaN contact layer.	172
Figure 7.50	The output power of MD-SLS InGaN DQWs LDs with n-AlGaN and n-GaN layers as a function of forward current.	172
Figure 7.51	Schematic diagram of the preliminary InGaN/GaN strained SQW LD.	175
Figure 7.52	The bandgap profile and the carrier density of InGaN strained SQW LD.	176
Figure 7.53	The blue shift in laser peak wavelength as a function of forward current due to polarization and the screening in the internal electric field of InGaN strained SQW LD.	177
Figure 7.54	The internal electric field of InGaN strained and unstrained SQW LDs.	178
Figure 7.55	The output power of InGaN strained and unstrained SQW LDs.	178
Figure 7.56	The reduction in the threshold current for strained SQW of InGaN LD.	179
Figure 7.57	The slope efficiency and DQE as a function of strain for InGaN SQW LD.	179

LIST OF ABBREVIATIONS

III-V material	Material, typically crystalline, composed of roughly equal parts of elements from group –III of the periodic table and elements from group-V of the periodic table
LD	Laser Diode
QW	Quantum Well
SCH	Separate Confinement Heterostructure
SLS	Strained Layer Superlattice
DH	Double Heterostructure
MQW	Multi Quantum Well
HVPE	Hydride Vapor Phase Epitaxy
MOCVD	Metal Organic Chemical Vapor Deposition
FWHM	Full Width at Half Maximum
GaN	Gallium Nitride
FP	Fabry-Perot
EEL	Edge Emitting Laser
VCSELs	Vertical Cavity Surface Emitting Lasers
LED	Light Emitting Diode
DBR	Distributed Bragg Reflector
DFB	Distributed Feedback
NFP	Near Field Pattern
FFP	Far Field Pattern
QCSE	Quantum Confined Stark Effect
MOCVD	Metalorganic Chemical Vapour Deposition
MBE	Molecular Beam Epitaxy
DQE	External Differential Quantum Efficiency
ISE TCAD	Integrated System Engineering Technology Computer Aided Design
FEM	Finite Element Method
SQW	Single Quantum Well

LIST OF SYMBOLS

E_F	Fermi energy (eV)
ξ	Electric field (V/cm)
E_g	Band gap (eV)
E_V	Valence band edge (eV)
h	Planck's constant (6.626×10^{-34} J.s)
I	Current (A)
J	Current density (A/cm^2)
k	Boltzmann's constant (8.617×10^{-5} eV/K)
m	Electron mass (9.11×10^{-31} kg)
m^*	Effective mass (kg)
m_n	Electron effective mass (kg)
m_p	Hole effective mass (kg)
n	Index of refraction
n_R	Index of refraction in material
N_A	Acceptor doping density (cm^{-3})
N_C	Effective density of states in the conduction band (cm^{-3})
N_D	Donor doping density (cm^{-3})
N_V	Effective density of states in the valence band (cm^{-3})
N_h	Hole concentration (cm^{-3})
N_e	Electron concentration (cm^{-3})
N_{eff}	Effective carrier concentration (cm^{-3})
N_s	Interfacial state density
p	Hole density (cm^{-3})
μ_n	Electron mobility ($cm^2/V.s$)
μ_p	Hole mobility ($cm^2/V.s$)
g_{th}	Threshold gain
Γ	Confinement factor
α_i	Internal loss
α_m	Loss due to the mirrors or facets

R_1, R_2	Laser mirror reflectivities
L	Laser cavity length
q	Electron charge
n_{th}	Threshold carrier concentration
B_{12}	Einstein coefficient for absorption
τ	Carrier lifetime
d	Thickness of the active layer
R_{sp}	Spontaneous emission rate
α	Total loss
η_{int}	Internal efficiency
η_{ext}	External quantum efficiency
I_{th}	Threshold current
η_d	External differential quantum efficiency
J_{th}	Threshold current density
J_0	Transparency threshold current density
T_0	Characteristic temperature
C_p	Specific heat
κ	Thermal conductivity
SRH	Shockley–Read–Hall
λ	Wavelength.

REKABENTUK DAN PRESTASI STRUKTUR LASER BERASASKAN KUMPULAN III-NITRIDA

ABSTRAK

Simulasi peranti bagi ciri elektrik, optik dan terma diod-diod laser (LDs) berasaskan GaN telah dikaji. Bagi laser-laser sedemikian adalah susah memperoleh lapisan penutup-p yang mempunyai ketebalan yang mencukupi, yang berkomposisi Al tinggi dan berketumpatan penerima yang tinggi. Ini menghasilkan aliran lebih elektron-elektron dari rantau aktif ke lapisan penutup-p yang menghasilkan kesan ketara ke atas peningkatan ketumpatan arus ambang. Maka, rekabentuk peranti bagi lapisan strukturnya adalah sangat penting supaya menghasilkan laser-laser ambang rendah. Ciri-ciri terma adalah juga sangat penting bagi laser-laser berasaskan GaN. Keputusan analisis terma menunjukkan bahawa pengurangan ketumpatan arus ambang dan voltan operasi adalah penting bagi menambahbaik ciri suhu laser-laser semikonduktor GaN.

Dalam kajian ini rekabentuk struktur LDs InGaN termasuk peranti rantau aktif perigi kuantum multi (MQW) telah diperihal dan dikaji menggunakan simulator “Integrated System Engineering Technical Computer Aided Design“ (ISE TCAD). Parameter-parameter struktur LDs diubah dan dioptimumkan bagi menghasilkan prestasi tinggi. Kajian pengoptimuman ini merangkumi aspek-aspek seperti ketebalan rantau aktif, pendopan, ketebalan rantau lapisan penghenti, ketebalan perigi dan sawar kuantum, bilangan perigi kuantum dan beberapa pendekatan bagi penambahbaikan dan perolehan kecekapan tinggi, arus ambang rendah dan kuasa keluaran tinggi bagi LDs InGaN. Struktur LDs asas yang dikaji adalah jenis Fabry-Perot InGaN heterostruktur berpasangan (DH), heterostruktur pengurangan berasingan (SCH) dan struktur perigi kuantum multi (MQW).

Berasaskan keputusan-keputusan kajian, kuasa keluaran 84 mW dan arus ambang 110 mA diperolehi bagi struktur LD DH. Anjakan biru bagi panjang gelombang pancaran laser dari 428 nm ke 426.2 nm telah dapat diperhatikan. Bagi LD InGaN tunggal seperti pukal, kuasa keluaran 97 mW dan nilai ambang arus 90 mA telah diperolehi. Terdapat kesan-kesan yang kuat ke atas prestasi laser dengan kehadiran dan tanpa kehadiran lapisan penghenti.

LDs prestasi tinggi diperolehi menggunakan perigi kuantum multi yang dikenakan dengan parameter-parameter yang telah dioptimumkan. Arus ambang paling rendah, kecekapan kuantum luaran dan suhu cirian yang lebih tinggi diperolehi apabila bilangan lapisan perigi InGaN adalah dua pada pancaran laser dengan panjang gelombang 415 nm, yang dikaitkan dengan permasalahan pembawa-pembawa inhomogen.

Penambahbaikan prestasi laser dan suhu cirian telah juga diperolehi menggunakan sawar kuantum multi (MQBs) AlGa_{0.3}N/GaN di dalam diod laser InGa_{0.5}N/GaN. Arus ambang bernilai 10.9 mA, kuasa keluaran dan kecekapan kecerunan masing-masing bernilai 17.42 mW dan 1.6 W/A, dan suhu cirian bernilai 307 K telah diperolehi. Semua ini dikaitkan dengan pengaruh sawar yang tinggi di dalam MQBs yang menghalang kebocoran pembawa dari rantau aktif. Juga telah dicerapkan bahawa perigi kuantum tunggal (SWQ) InGa_{0.5}N/GaN bertegasan dapat mengurangkan arus ambang dari nilai 18.5 mA ke 14.5 mA dan kuasa keluaran ditingkatkan dari 15 mW ke 28 mW dan menambahbaikan prestasi laser jika dibandingkan dengan yang tanpa tegasan.

DESIGN AND PERFORMANCE OF LASER STRUCTURES BASED ON GROUP III-NITRIDES

ABSTRACT

Device simulations for the electrical, optical and thermal characteristics of GaN-based laser diodes (LDs) have been investigated. It is difficult to obtain p-cladding layers with sufficient thickness of high Al composition and high acceptor concentration, this causes electrons overflow from the active region to the p-cladding layers which has significant effects on the increase in the threshold current density. Therefore, the device design for the layer structure is very important in order to realize low-threshold lasers. Thermal characteristics are also very important for GaN-based lasers. The results of thermal analysis indicate that the reduction in the threshold current density and operation voltage is very important for improving the temperature characteristics of GaN semiconductor lasers.

In this work the design of InGaN LDs structures including multi quantum wells (MQWs) active region device are described and investigated by integrated system engineering technology computer aided design (ISE TCAD) device simulator. The parameters of the LDs structures are varied and optimized for high performance. This optimization study involves aspects such as thickness of active region, doping, thickness of stopper layer region, thickness of quantum wells and quantum barriers, number of quantum wells and several approaches to improve and achieve high efficiency, low threshold current and high output power of InGaN LDs. The basic LDs structures treated here are Fabry–Perot type InGaN double heterostructure (DH), separate confinement heterostructure (SCH) and multi quantum wells (MQWs)

Based on our results, output power of 84 mW and threshold current of 110 mA are obtained from DH LD structure. A blue shift for the laser emission wavelength from 428 nm to 426.2 nm are also observed. In InGaN single bulk like LD, output power value of 97 mW and threshold current value of 90 mA are obtained. There are strong effects was observed with the presence and absence of the stopper layer on the laser performance.

High performance LD has been obtained by using multi quantum wells incorporated with the optimized parameters. The lowest threshold current, higher external quantum efficiency and characteristic temperature are obtained when the number of InGaN well layers is two, at our laser emission wavelength of 415 nm, which is related to the problem of inhomogeneous carrier.

An improvement in laser performance and characteristic temperature has been achieved using AlGaIn/GaN multiquantum barriers (MQBs) in InGaIn/GaN laser diodes. Threshold current value of 10.9 mA, output power and slope efficiency of 17.42 mW and 1.6 W/A respectively and characteristic temperature of 307 K are obtained. These are attributed to the influence of the high barriers in the MQBs in preventing carrier leakage from the active region. It is also observed that the InGaIn/GaN strained single quantum well (SQW) LD reduced the threshold current from the value of 18.5 mA to 14.5 mA and the output power increases from 15 mW to 28 mW and improved the laser performance as compared with their unstrained counterparts.

CHAPTER 1

INTRODUCTION

1.1 Overview

The first semiconductor laser diodes (LDs) were made by heavily doping a p-n junction and then cleaving reflecting facets at either end of its Fabry-Perot resonant cavity (Mroziwicz *et al.*, 1991). This design is less efficient than the double heterostructure (DH) and multi quantum wells (MQWs) designs that would follow since, in a p-n junction, there is no clearly defined region where recombination takes place. Carriers can easily be lost to diffusion before recombination can occur. This means a high threshold current is necessary to achieve stimulated emission and lasing. Threshold currents were reduced with the development of the DH LD.

The DH consists of a narrow bandgap material sandwiched between two wider bandgap materials. This forms a quantum well (QW) which very effectively confines carriers within the well when forward biased. This is advantageous since the carriers tend to remain there until they recombine. It thus became possible to control where the radiative transitions would occur within the device. The DH has a secondary advantage in that the wider bandgap materials tend to have lower indices of refraction. This means that they act as cladding layers to guide the light propagating through the active layer. The addition of a stripe contact to the top surface of the device allows for the current flow to be confined to a small region of the device. The cavity is formed by cleaving the semiconductor along a crystal plane using a diamond scribe.

The advent of the multi quantum wells (MQWs) LD further enhanced carrier confinement. In a MQWs LD, carriers are confined in a series of thin quantum wells

(also called superlattices for small enough scales). Additionally beneficial, emission spectra can be tuned by varying the width of the quantum well layer since the thickness of a quantum well determines the eigenvalues allowable in the well (and the eigenvalues determine the transition energies). Here we briefly identify some of the benefits of DH and MQW LDs versus their bulk laser counterparts:

The DH/MQWs LDs achieve larger gain for a low concentration of injected carriers. This also implies a low transparent current density. DH/MQWs LDs achieve a larger differential gain. This allows a higher speed of operation which is vital to applications in the telecommunications industry. Also, DH/MQWs LDs split the light and heavy hole energy bands, which allows control of optical polarization (Zory, 1993). In addition, DH/MQWs LDs have much narrower gain spectra. This improves device efficiency and optical coupling.

The development of blue light emitting semiconductor devices involved many challenges. Akasaki, Amano and Nakamura, respectively, succeeded in overcoming these challenges through highly creative approaches within the same time frame (Takeda Award 2002 Achievement Facts Sheet). Akasaki was confident that gallium nitride (GaN) would be the best material with which to make blue light emitting semiconductor devices, although the majority of researchers were using zinc selenide (ZnSe). Akasaki and Amano fabricated GaN film with good crystal quality and uniform thickness on an aluminum nitride (AlN) buffer layer grown on a sapphire substrate. Then, they fabricated a p-type GaN layer with high conductivity by using electron beam irradiation on a p-type impurity doped GaN thin film. In 1989, they developed a p-n junction blue light emitting diode (LED) in their laboratory. They observed emission of strong blue light with a narrow bandwidth, and it was reported in November 1995. Nakamura also chose to work with GaN,

rather than with ZnSe used by the majority of researchers. He invented film deposition equipment with a unique two-flow method, and fabricated GaN film with good crystal quality and uniform thickness. He achieved high conductivity, p-type GaN by heat treatment in the atmosphere without hydrogen. He developed a high brightness blue light emitting diode (LED) of double heterostructure using In-doped GaN layer in 1993. He succeeded in achieving laser oscillation by introducing a multi-quantum well structure with several tens of InGaN layers and a blocking layer, and reported this in January 1996. Figure 1.1 shows the timeline activities of GaN over the years and some of its applications.

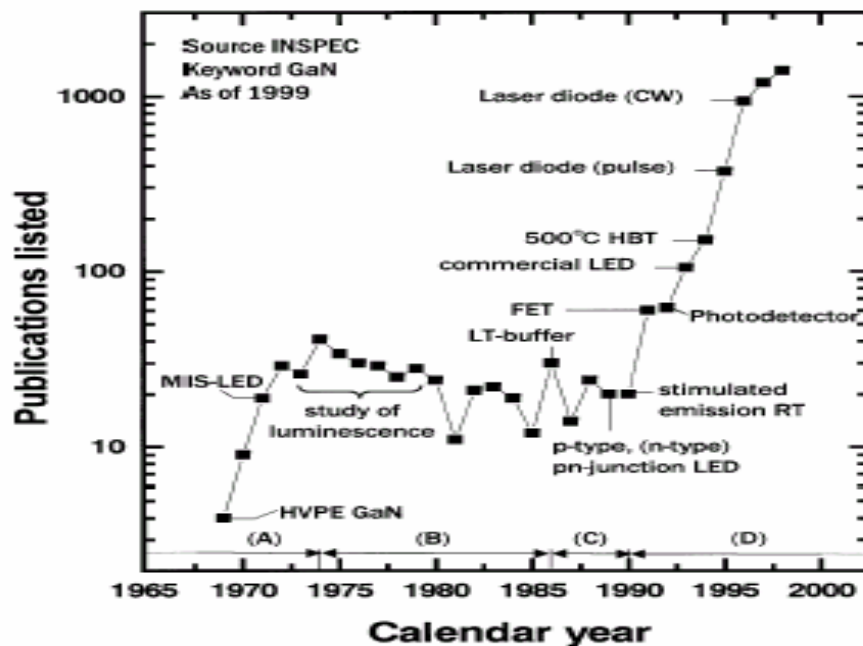


Figure 1.1: Number of publications (INSPEC) and activities in GaN over the years (Akasaki, 2002).

Based on these achievements, the blue LED was introduced in 1993 and the blue LD was introduced in 1999. Those were the first blue LED and blue LD commercialized products in the world. Akasaki, Amano and Nakamura overcame

difficult challenges that required a creative approach. Moreover, they contributed to the commercialization of blue LD and LED-based devices. The Takeda Award 2002 for Social/Economic Well-Being is awarded to this techno-entrepreneurial achievement that embodies engineering intellect and knowledge, and enables many applications in human life that will expand the wealth, richness, and happiness of people.

Akasaki undertook research to develop blue light emitting devices using GaN in the 1970s. He adopted a molecular beam epitaxy (MBE) method that can bond each molecule to the right place, in addition to the previously used hydride vapor phase epitaxy (HVPE) method. He succeeded in fabricating a GaN single crystal film using MBE method. In 1981, he achieved light emission from a metal-insulator semiconductor structure with 0.12% efficiency using HVPE method (Ohki *et al.*, 1981).

However, he could not develop a thin film with good thickness uniformity. Also, he could not produce a p-type GaN film. Even on this macroscopically inferior quality crystal, he noticed a strong light emission from the very small spot of film that had thickness uniformity. This observation convinced him that GaN was, indeed, the material with which to develop a blue light emitting device, despite the fact that many other researchers had abandoned GaN-based research. In 1981, Akasaki moved to Nagoya University to continue his research. In 1982, Amano joined Akasaki's laboratory and began his research work.

Akasaki had recognized the limitations of the HVPE method and the MBE method for GaN thin film fabrication. The problem with the HVPE method is that the crystallinity of thin film is bad under high speed of film fabrication. While the problems associated with the MBE method include slow film fabrication speed and

the difficulty in attaining a stoichiometric composition. This is a script to the nitrogen which is easily pulled out by its high vapor pressure in an ultra-high vacuum ambient atmosphere. He decided to use a metal organic chemical vapor deposition method (MOCVD method) that brought an appropriate film fabrication speed in the same temperature region for each film. He selected a sapphire substrate, which can be used at a GaN film fabrication temperature of over 1,000 °C in MOCVD method, and has lattice symmetry near to that of GaN. However, because the lattice constant difference was 16 percent, it was a difficult challenge to fabricate hetero epitaxial thin film with good crystal quality and thickness uniformity.

Akasaki and Amano designed and developed the MOCVD equipment by themselves, because MOCVD fabrication equipment that could be used for GaN was not available at that time. They tried to identify the best fabrication conditions by repeating experiments with various combinations of substrate temperature, vacuum pressure, material gas feed rate, inactive gas feed rate, fabrication time length, and so on. They performed over 1,500 experiments in two years, but they could not fabricate thin film with good crystal quality and thickness uniformity. They conceived of locating a buffer layer fabricated at low temperature between the sapphire substrate and the GaN thin film after thorough investigation of their experimental results. They selected GaN, aluminum nitride (AlN), SiC, and zinc oxide as the candidates. They succeeded in fabricating GaN thin film with good crystal quality and thickness uniformity using AlN as a buffer layer in 1986 (Amano *et al.*, 1983). Good crystal quality of the film was confirmed using photoluminescence, X-ray diffraction, Hall effect measurement, transmission electron microscope and so on. From the result of Hall effect measurement, the electron mobility at room temperature was calculated to be improved from

50 cm²/V.s to 450 cm²/V.s (Akasaki *et al.*, 1989). Moreover, they succeeded in realizing the n-type thin film with thickness uniformity and good conductivity (Amano and Akasaki, 1990). This success was achieved not just through one experiment, as above, but instead required a tremendous number of experiments to find the optimized conditions that made it a great breakthrough.

GaN thin films usually became n-type semiconductors, because they contained smaller stoichiometric numbers of nitrogen. Attempts were made to make a p-type layer using acceptor-doping material. This was also a big hurdle to making a GaN light emitting device. Akasaki and Amano initially used zinc as an acceptor dopant and tried to fabricate p-type GaN, but they did not achieve success. After they used magnesium as a dopant because of its higher electron affinity, they still did not achieve success. In 1988, Amano found that cathode luminescence light intensity increases with electron beam irradiation in other experiments to measure cathode luminescence of acceptor doped GaN. He thought from this result that the electrical and optical characteristics of acceptor doped GaN thin film was changed by electron beam irradiation (Amano *et al.*, 1988).

Based on this, they measured the electrical characteristics of 10 kV electron irradiated Mg doped GaN thin film and found that the resistivity decreased by a factor of 10,000 to 35 Ohm-cm, and confirmed that GaN film is clearly p-type by its Hall effect measurement. Its hole mobility was 8 cm²/V.s. They made a p-n junction at the same time and measured current rising in the forward direction on the current-voltage curve and light emission both are characteristics of p-n junction (Amano *et al.*, 1989). This p-type layer fabrication method by electron beam irradiation was the historic first fabrication of p-type GaN. They made an important step toward developing a blue light emitting semiconductor device by inventing p-

type GaN fabrication and GaN layer fabrication method. From 1987, Akasaki and Amano led blue LED development at Toyoda Gosei Co. Ltd.; they received funding from the Japan Science and Technology Corporation. In 1992, they succeeded in developing a bright blue LED with 1 percent light emitting efficiency. Toyoda Gosei announced commercial production of blue LEDs in 1995.

Akasaki and Amano also undertook the challenges of developing a blue LD. In 1990, they succeeded in measuring narrow bandwidth 374 nm stimulated emission at room temperature with high density electron-hole pairs created by radiating 337nm nitrogen laser beam on a GaN thin film, which was fabricated on a low temperature buffer layer with good thickness uniformity (Amano *et al.*, 1990). They fabricated a multi-quantum well structure device which is decreasing the laser diode threshold power density. They succeeded in measuring strong emission of 3nm half bandwidth on 1.0 kA/cm injection current density, which they reported in Japanese Journal of Applied Physics in November 1995 (Akasaki *et al.*, 1995). They reported achieving a laser oscillation of 405nm wavelength in June 1996 (Akasaki *et al.*, 1996).

Shuji Nakamura began development of a blue light emitting semiconductor device at Nichia Chemical Industries, Ltd., in 1988. In order to undertake this research, he had to obtain the consent of the president of Nichia Chemical Industries through direct negotiation, something that was extraordinary for a researcher in a Japanese company to do. Material selection was an important issue. Since many researchers were pursuing ZnSe-based blue LED research and would patent their manufacturing technology processes, Nakamura decided it would be difficult to develop a novel technology. Therefore, he selected GaN as the focus of his research, which was only being pursued by a minority of researchers. Nakamura had the

confidence and engineering creativity to solve the technical problems stemming from GaN-based research.

Nakamura began his experiment to make GaN thin film using standard equipment with a well-known substrate material, sapphire, and a well known method, MOCVD. However, GaN thin film with good uniformity had yet to be produced. Nakamura thought that the gas flow scheme was the key issue to improving film uniformity. This approach is different from that taken by Akasaki and Amano, who introduced the low-temperature buffer layer. Nakamura thought over many kinds of gas flow schemes that were different from the conventional layer flow. In the conventional gas flow, material gases, including Ga compound and nitrogen, were supplied in parallel to the substrate surface as the layer flow.

This conventional scheme was considered to be rational but had achieved only inferior uniformity and less than stoichiometric nitrogen content. Nakamura repeatedly modified the MOCVD equipment by himself to change the gas flow mode, and performed experiments over 500 times in a short period. Finally, he found the most appropriate method where the main material gases, including Ga compound, flow in parallel to the substrate, and nitrogen and hydrogen are supplied vertically from the upper side to the substrate surface. In 1991, he succeeded in fabricating a GaN thin film with superior uniformity using this method, which he named the “two-flow method” (Nakamura *et al.*, 1991a). The electron mobility calculated from the Hall effect measurement with this GaN thin film was $200 \text{ cm}^2/\text{V}\cdot\text{s}$, which was much larger than the conventional result of $90 \text{ cm}^2/\text{V}\cdot\text{s}$. In an additional experiment, in which the low temperature buffer layer was introduced as well as the two flow method, the resultant GaN thin film showed $500 \text{ cm}^2/\text{V}\cdot\text{s}$, which is a satisfactory figure for light emitting device fabrication. Moreover, in 1992, he achieved high

quality InGaN ternary compound thin film by the two flow method. This film was necessary to optimize the emitted light wavelength and to improve the emission efficiency (Nakamura and Mukai, 1992).

Nakamura reexamined the material for the low-temperature buffer layer and found that not only AlN but also GaN itself was suitable (Nakamura, 1991b). In the case of GaN, the material gas change is not needed between the buffer layer and the active layer. This is practically important and beneficial for mass production technology. In order to fabricate the p-type GaN layer, Nakamura investigated another more practical method than that with electron irradiation studied by Akasaki and Amano. Heat treatment, using a specimen doped with magnesium as the acceptor impurity, had been studied but had proven unsuccessful. Nakamura reexamined the heat treatment effect and found that a hydrogen-free atmosphere was essential to activate the doped magnesium and get the p-type layer. He clarified the mechanism of p-type formation, proposing a model based on the connection between hydrogen atoms and acceptor impurities (Nakamura, 1992). Using this method, in 1992, the specific resistance of heat-treated GaN thin film was improved to 2 Ohm-cm smaller than usual by more than a factor of 100,000 and the superior p-type layer was successfully obtained where the hole mobility by Hall measurement was $10 \text{ cm}^2/\text{V}\cdot\text{s}$.

Using the above-mentioned technologies, Nakamura fabricated p-n homo junction blue LEDs with 0.18 % light emitting efficiency and the double heterostructure type with 0.22 % light emitting efficiency in 1992. The latter one was improved to 2.7 % light emitting efficiency using the above mentioned InGaN thin film as the light emitting layer, in 1993 (Nakamura *et al.*, 1994). Based on these results, Nichia Chemical Industries delivered the world's first blue LEDs in

1993. Moreover, the quantum-well structure was adopted to develop the high brightness blue LED with 9.2 % light emitting efficiency (Nakamura *et al.*, 1995).

Nakamura investigated the InGaN light emitting layer in detail. Before that time, to achieve a long light emission lifespan, the maximum allowable number of crystal defects was considered to be fewer than 10^3 cm^{-2} . Although there were many crystal defects about 10^{10} cm^{-2} in the InGaN film of LED, the lifespan of this LED was longer than 100,000 hours. The reason for this long lifespan with that level of defects is as follows. The distribution of indium atoms doped in GaN film is not uniform but fluctuates slightly, and consequently the potential for electrons in the crystal is not uniform but varies locally. Injected electrons are trapped in this localized potential and recombined with holes to emit the light without being captured by the crystal defect region. This kind of localized potential was a thoroughly new phenomenon not found in any previous crystal material and found first in this ternary mixed crystal InGaN. The research project then started intentionally to design and to make this kind of localization in the crystal.

Based on these technologies for GaN-based blue LEDs, Nakamura succeeded in achieving high power pulse oscillation of the GaN-based blue LD with an InGaN multi-quantum well structure and cladding layers. This was reported in the January 1996 issue of Japanese Journal of Applied Physics (Nakamura *et al.*, 1996). The key step for achieving this LD oscillation was introducing InGaN twenty cycle's multi-quantum well structure for the light emitting layer and AlGaIn film for blocking layer

In the case of LDs, compared to LEDs, the number of defects had to be decreased still more to obtain a long lifespan, since the number of injected electrons in LDs is larger. Nakamura adopted the epitaxial lateral overgrowth (ELOG) method (Usui *et al.*, 1997). In 1998, he succeeded in decreasing the defects from 10^{10} cm^{-2} to

10^7 cm^{-2} and achieved 290 hours of continuous oscillation at room temperature, from which the oscillating lifespan was estimated to be 10 thousand hours. In 1999, Nichia Chemical Industries delivered the world's first blue LD (Nakamura *et al.*, 2000).

1.2 Research Background

The first demonstration of a GaN based blue laser diode by Shuji Nakamura was followed by a tremendous research and development effort around the world. Gallium nitride technology enables a range of novel applications with vast consumer markets. Examples are full color video displays, solid-state lighting, and high-definition DVD players. However, there still remains a strong need for a more detailed understanding of microscopic physical processes in nitride devices. Advanced models and numerical simulation can help to investigate those processes and to improve the device performance.

1.3 Objectives of Study

We analyze the performance of nitride Fabry-Perot InGaN laser diodes theoretically using advanced laser software simulator. The vertical carrier leakage, lateral current spreading are some of the major problems because the reduction of such carrier losses is important to achieve less self heating and higher output power. Also, the effects of the inhomogeneous carriers distribution in the quantum well and the internal fields due to polarization on the laser diode performance are crucial issue that need to be investigated and solved. The important operating parameters of InGaN LDs such as internal quantum efficiency (η_i), the internal loss α_i , characteristic temperature (T_0) and the transparency current density J_0 are the key parameters which control the operating characteristics of LD. These parameters will be calculated and investigated for InGaN laser structures designed in this study.

1.4 Out Line of Thesis

Briefly, the content of this thesis are presented as follows:

Chapter 1 described the history of growth and the development of III- nitride material and its application for some optoelectronics devices such as LED and LD.

Chapter 2 explains in general the basic theories and concepts of laser diode and the related subjects in this work.

Chapter 3 describes the simulator itself and discusses the procedures involved in simulating LD structure. Several selected models used in simulating LD designs were also described.

Chapters 4, 5, 6 and 7 present the outcome of this research work. The LD performance on different design structures and various parameters variation are presented, analyzed and discussed. The results of these performance properties of our study will be compared with some of experimental work obtained from other researchers.

Chapter 8 will conclude the outcome in this study summarily. A few recommendations for further works also will be proposed in this chapter.

CHAPTER 2

THEORY

2.1 Introduction

This chapter explains the semiconductor laser diode theory and operation followed with the basic properties of Indium Gallium Nitride (InGaN) laser diode and its related materials generally. The discussions on several problems in LD device semiconductor and several approaches to overcome those problems in improving the LD performance are also presented. The basic principle of carriers in semiconductor devices is also explained. This principle describes the carriers' behavior and movement in LD device.

2.2 Background: Semiconductor Laser Theory and Operation

There exists a wealth of literature covering the various types of semiconductor laser, the physics of their operation, and their implementations and applications. Whilst the concepts described in this section are readily available in any of the aforementioned texts, the fundamental principles of laser action and an overview of the theory behind semiconductor laser diodes are provided in this chapter for convenience and completeness (Bhattacharya, 1997; Agrawal, 1993).

Specific details of some of the mathematical equations upon which the electrical semiconductor models are based will be provided. The concept of the semiconductor laser is based on the emission of a photon when a hole and electron recombine. Taking the case of a non-degenerate semiconductor at 0 K, all of the electrons lie on the valence band whilst the conduction band is empty. Pumping the semiconductor raises some electrons to the conduction band where they rapidly distribute themselves into the lowest available energy levels within the band.

Electrons in the valence band occupy the lowest energy levels there, pushing the holes to the top of the valence band.

2.2.1 Absorption

The processes that can occur in semiconductor lasers are shown in Fig. 2.1. Coordinating these processes are vital to the operation of a semiconductor laser diode (LD). In the first process, an incident photon excites a valence band electron into the conduction band. However, not all of the photons are absorbed. The absorption is governed by an absorption rate of the form,

$$R_{abs} = B_{12} \cdot p_1 \cdot (1 - p_2) \cdot \rho(\hbar\omega) \quad (2.1)$$

where p_1 and p_2 are the occupation probabilities in the valence and conduction bands respectively, B_{12} is the Einstein coefficient for absorption, and ρ is the density of photons equal to the transition energy.

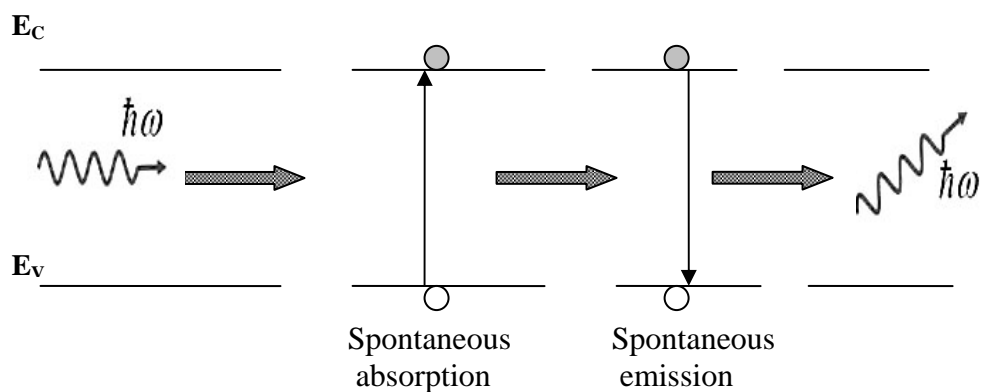


Figure 2.1: The mechanism of the spontaneous absorption and emission.

2.2.2 Spontaneous emission

In LDs, light is first produced by spontaneous emission as shown in Fig. 2.1, where electrons in the conduction band spontaneously recombine with holes in the valence band to emit photons of equal energy (Thompson, 1980; Sands, 2004):

$$E_{electron} - E_{hole} = E_g = h\nu \quad (2.2)$$

This initial emission (below threshold) then induces stimulated emission. LEDs, on the other, rely solely on spontaneous emission for device performance. All electron-hole pairs are independent. Hence, all photons are incoherent wave trains emitted in all directions. The rate of spontaneous emission, R , is proportional to the product of electron and hole concentrations.

$$R = -\frac{dn}{dt} = -\frac{dp}{dt} = Bnp \quad (2.3)$$

Here, n is the concentration of free electrons, p is the concentration of holes, and B is the bimolecular recombination coefficient. This can also be expressed in terms of the equilibrium carrier concentrations (n_0, p_0) (Svelte, 1998).

$$R = B(n_0 + p_0)\Delta n(t) \quad (2.4)$$

The rate of change in concentration, $\Delta n(t)$, is an exponential with a characteristic rise time equal to the carrier lifetime τ , and Δn_0 is the steady state excess electron concentration.

$$\Delta n(t) = \Delta n_0 e^{-B(n_0 + p_0)t}, \quad \tau = \frac{1}{B(n_0 + p_0 + \Delta n)} \quad (2.5)$$

2.2.3 Stimulated emission in semiconductors

If an incident photon “couples” with an electron it can cause the electron to fall back into the valence band. This “coupling” is somewhat analogous to sympathetic resonance in mechanical or acoustical systems where an incoming photon (emitted via spontaneous emissions) resonantly couples with an energized electron of the same frequency and phase as shown in Fig. 2.2. As the electron falls to the valence band it emits a photon. It is vital to the operation of LDs that the emitted photon is coherent with the incident photon; it has the same direction and phase. The rate of this stimulated emission is dictated by a process completely analogous to stimulated absorption, only this time there is a stimulated emission constant B_{21} which relates to transitions from the conduction to the valence band (Svelto, 1998; Siegman, 1971).

$$R_{emission} = B_{21}P_1(1 - P_2)\rho(\hbar\omega) \quad (2.6)$$

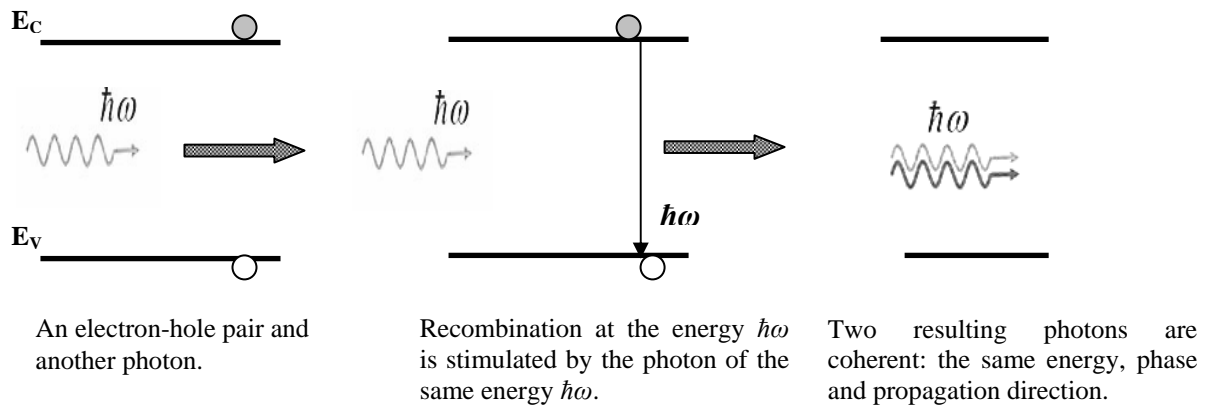


Figure 2.2: Process of stimulated recombination in laser diode.

These processes are really just reverses of each other; stimulated emission is the reverse of stimulated absorption, with the added advantage that stimulated emission multiplies the number of photons and thus provides gain. Probability of stimulated emission is proportional to the density of excess electrons and holes, and to the density of photons. Each time the number of photons is increased (amplified) we provide positive feedbacks that make the stimulated emission to become self supporting. The self supporting stimulated emission is the principle of a laser.

2.2.4 Einstein relations and population inversion

All the three of the processes described above (absorption, spontaneous emission, and stimulated emission) are related. This interrelation helps us understand the process of lasing. Consider a system with two energy levels E_1 and E_2 . In equilibrium, the rate of upward transitions must equal the rate of downward transitions, and the populations of each energy level (N_1 , N_2) are related by Boltzmann statistics:

$$\frac{N_1}{N_2} = \frac{g_{D1} \exp\left(\frac{-E_1}{kT}\right)}{g_{D2} \exp\left(\frac{-E_2}{kT}\right)} = \frac{g_{D1}}{g_{D2}} \exp\left(\frac{E_2 - E_1}{kT}\right) = \frac{g_{D1}}{g_{D2}} \exp\left(\frac{h\nu_{12}}{kT}\right) \quad (2.7)$$

where g_{D1} and g_{D2} are the degeneracies of the levels (similar to density of states N_C and N_V) and indicate the number of subenergy levels within E_1 and E_2 .

We then define τ_{21} as the lifetime of carriers in the conduction band before spontaneous emission takes place, with $A_{21} = \tau_{21}^{-1}$ being the Einstein coefficient for spontaneous emission. Referring to equations (2.1) and (2.6), we can state that under thermal equilibrium (Sands, 2004; Bhattacharya, 1997).

$$B_{12} = \left(\frac{g_{D2}}{g_{D1}} \right) B_{21} \quad (2.8)$$

$$\frac{A_{21}}{B_{21}} = \frac{8\pi\nu^3 n_R^3}{c^3} = \frac{\hbar\omega^3}{\pi^2 c^2} \quad (2.9)$$

where equations (2.8) and (2.9) are known as the Einstein Relations. If the degeneracies are equal $g_{D1} = g_{D2}$, then $B_{12}=B_{21}$ where the light velocity in free space c is replaced by the light velocity in a crystal $\frac{c}{n_R}$. Examining equation (2.7), we note that in order for sustained stimulation emission to occur, N_2 must be greater than N_1 . Otherwise, the energized electrons with which incoming photons resonate will be depleted from the conduction band. $N_2 > N_1$ defines population inversion, and if we assume that $\tau_r = \tau_{21}$, then $A_{21} = \tau_r^{-1}$ and,

$$B_{21} = \frac{c^3}{8\pi\nu^3 n_R^3 \tau_r} = \frac{\lambda^3}{8\pi\tau_r} \quad (2.10)$$

2.3 Gain, Losses, and the Lasing Condition

Population inversion enables lasing action and optical gain in a semiconductor, and this population inversion is achieved by creating nonequilibrium populations of the carriers in the bands. These nonequilibrium populations result from minority carriers injected across a forward-biased junction. In a lasing medium, stimulated downward transitions (Eq. 2.6) represent gain, and stimulated upward transitions (Eq. 2.1) represent loss. The luminescence from a semiconductor represents its spontaneous emission spectrum, which has a definite width (Bhattacharya, 1997).

For lasing to occur, the gain must be greater than or equal to the loss at a photon energy within this spectrum (generally the peak wavelength). Because the laser is built in a resonant cavity, a significant photon density arises in a supported cavity mode. This spontaneous emission induces stimulated emission, and emitted photons stimulate even further recombination in a chain-reaction fashion. Since the photon density is highest at the peak energy, they stimulate the most transitions; this means that the output spectrum grows and narrows simultaneously. This is the onset of superradiance. Thus the two conditions for lasing are: First the gain must be at least equal to the losses in the medium. Second the radiation must be coherent. The directionality and coherence of emitted light is maintained by constructing the laser in a Fabry-Perot cavity waveguide. The electric and magnetic fields that dictate waveguide modes operate according to the following wave equations (derived from Maxwell's equations (Bhattacharya, 1997) :

$$\begin{aligned}\Delta^2 E + \omega^2 \mu \epsilon_0 \epsilon_r E &= 0 \\ \Delta^2 H + \omega^2 \mu \epsilon_0 \epsilon_r H &= 0\end{aligned}\tag{2.11}$$

For the light to be guided through the desired area of the material (i.e., the active regions), it is necessary to confine the waveguide modes using cladding layers. The waveguide design determines how the light will be guided, and the cladding layers determine how it will be confined. The confinement factor Γ is the percentage of guided light that “fits” within the active layer. We can then define a modal gain which is equal to the threshold gain g_{th} multiplied by the confinement factor Γ . This modal gain is a measure of the power transferred from the active region into the propagating mode (Bhattacharya, 1997).

$$\Gamma \cdot g_{th} = \alpha_i + \frac{1}{2L} \cdot \ln\left(\frac{1}{R_1 R_2}\right) = \alpha_i + \alpha_m \quad (2.12)$$

where α_i is the internal loss in the medium, and α_m is the loss due to the mirrors or facets (with reflectivities R_1 and R_2) that define the cavity length L .

The gain is amplified since the light being reflected between these two facets is in a gain medium. Eq. 2.12 defines the threshold condition for lasing. The value of n which Eq. 2.12 is true is the threshold carrier concentration n_{th} , where

$$n_{th} = \frac{d_m}{d} \left(\frac{8\pi\nu_0^2 g_{th} \tau_r \Delta \nu n_r^2}{c^2} \right) \quad (2.13)$$

where d_m is the thickness of the mode volume, and d is the thickness of the active layer. We can then also define the population inversion necessary to satisfy the lasing condition,

$$N_{th} = \left(\frac{8\pi\nu_0^2 g_{th} \tau_r \Delta \nu n_r^2}{c^2} \right) \quad (2.14)$$

We then define a threshold current density by,

$$J_{th} = \frac{qdn_{th}}{\tau_r} = qdR_{sp}(n_{th}) \quad (2.15)$$

where R_{sp} is the spontaneous emission rate per unit volume and d is the thickness of the active region. It will be seen that one tries to minimize J_{th} for the most efficient LD operation.

2.4 Transparency Condition

In a semiconductor LD, an interesting effect occurs just prior to stimulated emission: there exists an injected carrier density n_{nom} that makes the medium transparent. At this point, emission and absorption are balanced and the gain equals zero. Therefore, any incident photons cannot get absorbed and simply pass through the medium, rendering it transparent. It follows that there is a current density associated with this carrier injection; this is the transparency current density J_0 (Bhattacharya, 1997):

$$J_0 = \frac{qdn_{nom}}{\tau_r} \quad (2.16)$$

where n_{nom} is generally on the order of n_{th} , d is the thickness of the active region, q electron charge and τ_r is the radiative life time of the carriers. We see explicitly that the threshold and transparency currents density are related by,

$$J_{th} = \frac{\Gamma \cdot g_{th} + \alpha}{\alpha} J_0 \quad (2.17)$$

where α is the total loss.

2.5 Differential Gain, Internal Efficiency, External Quantum Efficiency, Differential Efficiency, and Output Power

The differential gain of the medium is defined as follows (Sands, 2004):

$$\frac{\partial g}{\partial n} = \frac{\alpha}{\Gamma \cdot n_{nom}} \quad (2.18)$$

The internal efficiency η_{int} of an LED is defined as the ratio of photons emitted from the active region to electrons injected into the LED. It is a function of the radiative τ_r and nonradiative τ_{nr} carrier lifetimes.

$$\eta_{\text{int}} = \frac{\tau_r^{-1}}{\tau_r^{-1} + \tau_{nr}^{-1}} \quad (2.19)$$

In GaN, the radiative lifetime is much shorter than the nonradiative lifetime, so most carriers can recombine to emit photons before encountering traps. For most calculations in mature material systems, it is acceptable to approximate $\eta_{\text{int}} \approx 1$. Further, we can generally neglect τ_{nr} since it is typically several orders of magnitude longer than τ_r . The external quantum efficiency η_{ext} of a device is defined as number of photons emitted into free space per second to the number of electrons injected into device per second and given in Eq. (2.20) below.

$$\eta_{\text{ext}} = \frac{P/h\nu}{I/q} = \eta_{\text{int}} \eta_{\text{injection}} \eta_{\text{extraction}} \quad (2.20)$$

where the injection efficiency is typically 100%, P is the laser power and I is the operating current. The differential efficiency is defined by (Bhattacharya, 1997),

$$\eta_{\text{diff}} = \eta_{\text{int}} \left(\frac{\ln\left(\frac{1}{R}\right)}{\alpha_i + \ln\left(\frac{1}{R}\right)} \right) \quad (2.21)$$

where α_i is the internal loss R is the mirrors reflectivity. Finally, the particular importance to the quality of a laser diode is the amount of power it produces.

This output power is given by,

$$P_{out} = A(J - J_{th}) \left(\frac{\eta_{int} h \nu}{q} \right) \left(\frac{\frac{1}{2L} \ln \left(\frac{1}{R_1 R_2} \right)}{\alpha_i + \frac{1}{2L} \ln \left(\frac{1}{R_1 R_2} \right)} \right) \quad (2.22)$$

where A is the LD contact stripe area and J is the device threshold current density,

L is the laser diode cavity length and R_1, R_2 are the reflectivity of left and right laser diode mirrors.

2.6 Semiconductor Laser Structures

All of the conditions described above to achieve lasing are accomplished by forward biasing the device. This injects carriers into the active region, where they recombine and begin the process of establishing a population inversion, thus leading to stimulated emission. Fig. 2.3 shows how the cleaved facets of the device act as mirrors. This establishes the Fabry-Perot resonant cavity which resonates at a frequency corresponding to the energy of the stimulated emission (Mroziewicz et al., 1991)

A Fabry-Perot cavity is required to provide the necessary optical feedback so that laser oscillation can occur. It can be established by polishing the end facets of the junction diode (so that they act as mirrors) and also by roughening the side edges to prevent leakage of light from the sides of the device (Vukovic, 2000). This structure is known as a homojunction laser. As a result of the difference in the refractive index and the difference in bandgap energies of the materials used, the heterojunction structure can considerably increase device efficiency. By using a heterojunction of either side of the active layer (Double Heterojunction (DH)

structure) both optical and carrier confinement are improved. The DH provides for optical confinement perpendicular to the junction, but confinement within the active layer is also desirable. The use of a stripe in the laser structure allows for optical confinement parallel to the active layer. The stripe essentially acts as a guiding mechanism by limiting current spread over the active layer. This is achieved by creating an area of high resistance over the region of the active layer in which lasing is to be suppressed which is a current blocking layer. The efficiency of the blocking layer will depend on its geometry and the current spread.

For a wave to exist within the cavity (of length L), it must be of an integer number of half wavelengths in length $L = n\lambda/2$, where λ is the wavelength of the light in the material. The spacing between the modes is given by $\Delta k = 2\pi / L$. Given that $L \gg \lambda$ there will be a large number of modes within the cavity and they will be closely spaced. Below threshold the emission of photons comes largely from spontaneous emission.

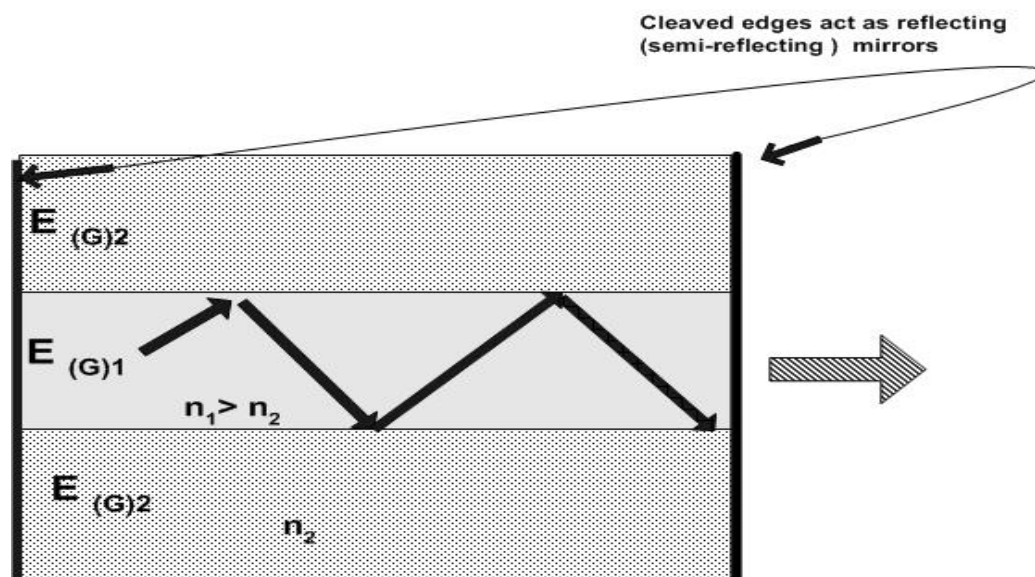


Figure 2.3: A schematic description of a Fabry-Perot resonant cavity with reflecting facets on each end.